Chem Soc Rev

TUTORIAL REVIEW

View Article Online
View Journal | View Issue

Cite this: *Chem. Soc. Rev.*, 2021, **50**, 6290

Fabrication of desalination membranes by interfacial polymerization: history, current efforts, and future directions

Xinglin Lu [ab] and Menachem Elimelech *[b]

Membrane desalination is a promising technology for addressing the global challenge of water scarcity by augmenting fresh water supply. Continuous progress in this technology relies on development of membrane materials. The state-of-the-art membranes used in a wide range of desalination applications are polyamide thin-film composite (TFC) membranes which are formed by interfacial polymerization (IP). Despite the wide use of such membranes in desalination, their real-world application is still hampered by several technical obstacles. These challenges of the TFC membranes largely stem from the inherent limitations of the polyamide chemistry, as well as the IP reaction mechanisms. In the past decade, we have witnessed substantial progress in the understanding of polyamide formation mechanisms and the development of new IP strategies that can potentially lead to the redesign of TFC membranes. In this Tutorial, we first present a brief history of the development of desalination membranes and highlight the major challenges of the existing TFC membranes. We then proceed to discuss the pros and cons of emerging IP-based fabrication strategies aiming at improving the performance of TFC membranes. Next, we present technical obstacles and recent efforts in the characterization of TFC membranes to enable fundamental understanding of relevant mechanisms. We conclude with a discussion of the current gap between industrial needs and academic research in designing high-performance TFC membranes, and provide an outlook on future research directions for advancing IP-based fabrication processes.

Received 19th January 2021

DOI: 10.1039/d0cs00502a

rsc.li/chem-soc-rev

Key learning points

(1) Current status of desalination processes and historical timeline for the development of desalination membranes.
(2) Major challenges of thin-film composite (TFC) membranes made by interfacial polymerization (IP) in desalination applications.
(3) Emerging strategies of IP for fabricating high-performance TFC membranes.
(4) Emerging techniques for polyamide thin-film characterization for revealing structural information of TFC membranes.
(5) Gap between industrial needs and academic research in designing high-performance TFC membranes, and potential research directions for advancing IP-based fabrication processes.

1. Introduction

Water is a precious resource, essential to humanity's sustainability and well-being.[1] However, population growth, industrialization, and water contamination have led to the pressing challenge of water scarcity around the globe.[2] Presently, over one billion people do not have adequate access to safe drinking water, and this figure is predicted to double in the coming decade. To address this global challenge, we need technological innovations to enable an efficient and sustainable supply of fresh water.

Desalination can offer a steady supply of high-quality fresh water through the treatment of seawater and brackish groundwater. These saline waters account for 97.5% of the water sources on our planet, making desalination an important solution to addressing water scarcity on a global scale.[3] To date, over 18 000 operational desalination plants provide ~90 million m^3 of fresh water daily to meet the demand of 300 million people, a number equivalent to the population of the United States.[4]

Growing interest in desalination has resulted in several technologies, which can be largely classified into two

[a] *CAS Key Laboratory of Urban Pollutant Conversion, Department of Environmental Science and Engineering, University of Science and Technology of China, Hefei 230026, China*
[b] *Department of Chemical and Environmental Engineering, Yale University, New Haven, Connecticut 06520-8286, USA. E-mail: menachem.elimelech@yale.edu*

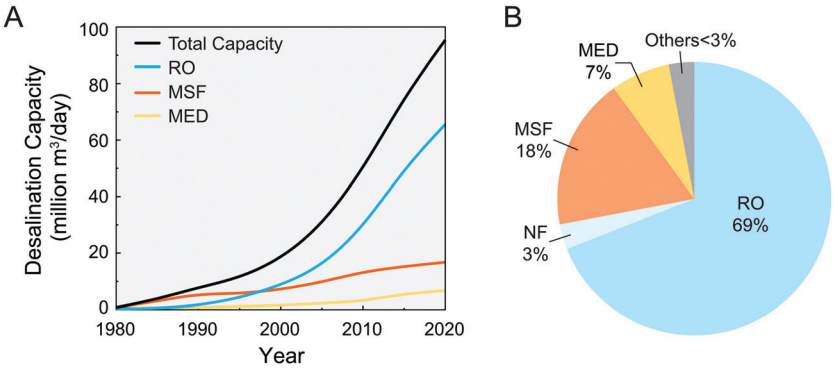

Fig. 1 Overview of the development and current status of desalination processes. (A) Trends in global desalination capacity in the past decades. (B) Share of operational facilities using different technologies, including reverse osmosis (RO), nanofiltration (NF), multi-stage flash (MSF), and multi-effect distillation (MED). Figures are reproduced with permission from ref. 6, Elsevier.

categories: thermal-based processes and filtration-based processes. Thermal-based processes exploit a thermal-driven phase change to separate water from non-volatile contaminants like salt. These processes, such as multi-effect distillation (MED) and multi-stage flash (MSF), were widely employed in the Gulf countries before the 1990s (Fig. 1A). Filtration-based processes, including reverse osmosis (RO) or nanofiltration (NF), rely on external pressure to drive water molecules across a semi-permeable membrane. Although both thermal-based and filtration-based processes are effective in producing fresh water, the intrinsic difference in driving force leads to different separation principles and energy-consumption levels, which were explained in a recent review article.[5] In brief, thermal desalination processes must overcome the enthalpy of vaporization (*i.e.*, latent heat, ΔH_{vap}), while the filtration processes must overcome the Gibbs free energy of separation (ΔG_{mix}). To produce a unit volume of fresh water under typical operating conditions, ΔH_{vap} is at least two orders of magnitude larger than ΔG_{mix} (667 *vs.* 1.06 kW h^{-1} m^{-3} for 50% water recovery). As a result, filtration-based processes consume much less energy than thermal-based processes in seawater desalination, despite measures to recover the latent heat of vaporization in thermal desalination technologies. Consequently, filtration-based RO has become the predominant destination technology, as illustrated by the rapid growth in the past two decades (Fig. 1A), accounting for ~70% of the global desalination capacity (Fig. 1B).[6]

The development of the RO process has largely been governed by advances in membrane materials, the core of the whole process. A chronological summary of the evolution of the RO desalination process is presented in Fig. 2 to illustrate the major milestones in the development of this technology. While the phenomenon of osmosis was first discovered in 1748, the proof-of-concept of RO desalination was not demonstrated until two centuries later, in the 1950s, using symmetric cellulose acetate films.[7] Despite good rejection of NaCl, the water flux of such films was too low to be practically viable. Later, in the 1960s, two pioneers—Loeb and Sourirajan—developed the first asymmetric cellulose acetate (CA) membrane *via* phase separation.[7] This membrane exhibited high salt rejection with ten times larger

Xinglin Lu

Xinglin Lu is a tenure-track assistant professor in the Department of Environmental Science and Engineering at the University of Science and Technology of China (USTC). He received his PhD from Harbin Institute of Technology under the supervision of Prof. Jun Ma, followed by postdoctoral training in Prof. Menachem Elimelech's group at Yale University. He is broadly interested in technologies that hold potential in addressing challenges at the water-energy nexus. His current research focuses on advanced membrane materials and processes for sustainable water supply and wastewater management.

Menachem Elimelech

Menachem Elimelech is the Sterling Professor of Chemical and Environmental Engineering at Yale University. His research interests include emerging membrane-based technologies at the water-energy nexus, materials for next generation desalination and water purification membranes, and environmental applications of nanomaterials. Professor Elimelech is a Clarivate Analytics (formerly Thomson Reuters) Highly Cited Researcher in two categories: chemistry and environment/ecology. He is a member of the US National Academy of Engineering and a foreign member of the Chinese Academy of Engineering.

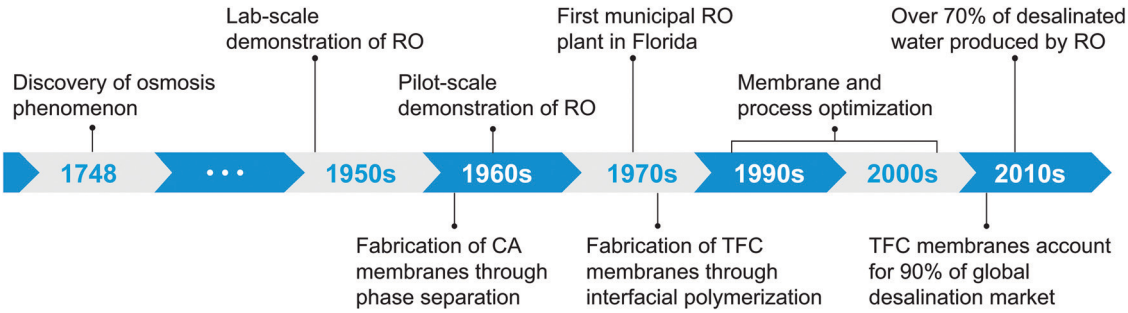

Fig. 2 Historical timeline of the development of membrane-based desalination processes.

water flux than that of any available membranes, thereby facilitating real-world applications of the RO process. Using this asymmetric cellulose acetate membrane, the first pilot-scale RO system was demonstrated in California in the 1960s, followed by the establishment of the first RO municipal plants in Florida in the 1970s.[7] These practical applications also enabled engineers and researchers to realize the shortcomings of the cellulose-type membranes in long-term operation, including a narrow operating pH range and susceptibility to biological degradation. To overcome these limitations, Cadotte developed the first thin-film composite (TFC) polyamide membranes in the late 1970s.[8] Compared with the cellulose acetate membranes, the TFC membrane is characterized by exceptional desalination performance (high water flux and high salt rejection) and enhanced stability under a wider pH range, thereby becoming the gold standard in RO-based desalination technologies.[3]

TFC membranes are fabricated through interfacial polymerization (IP)—a process that allows for the facile synthesis of an ultrathin selective layer. A representative procedure for fabricating TFC RO membranes is illustrated in Fig. 3. A microporous polysulfone membrane is first immersed in an aqueous diamine solution, *m*-phenylenediamine (MPD), to allow diamine penetration into the support. After removing the excess diamine on the surface, the impregnated support is brought into contact with an organic phase of acyl chloride—trimesoyl chloride (TMC). As MPD monomers diffuse to the interface between water and organic phases, they react with the TMC to form a thin polyamide layer on top of the polysulfone support.

Although the advent of TFC membranes resulted in remarkable energy savings in desalination, certain features of the fabrication procedure and film properties are inherently limiting. For example, the seemingly straightforward IP process turns out to be rather complex, limiting the fundamental understanding of polyamide formation mechanisms. As such, existing industrial fabrication processes are largely empirical and lack molecular-level design, leading to the formation of TFC membranes with uncontrolled characteristics. Some membrane characteristics lead to deleterious phenomena (*e.g.*, fouling and low rejection of neutral solutes) that are detrimental to product water quality and system efficiency. Given the dominant role of TFC membranes in RO desalination, there is a crucial need for a better mechanistic understanding of the IP process to enable innovative designs and to further advance RO desalination technologies.

Herein, we review the most recent progress in the IP process towards the fabrication of high-performance TFC membranes. We begin by highlighting the major limitations of TFC membranes regarding their fabrication process and real-world applications. We proceed to analyze the pros and cons of emerging IP-based fabrication strategies that aim at improving the robustness of TFC membranes. We then present technical obstacles and recent efforts in the characterization of TFC membranes to enable fundamental understanding of relevant mechanisms. Finally, we discuss the current gap between industrial needs and academic research in fabricating TFC membranes, and provide an outlook on future research directions for advancing IP-based fabrication processes.

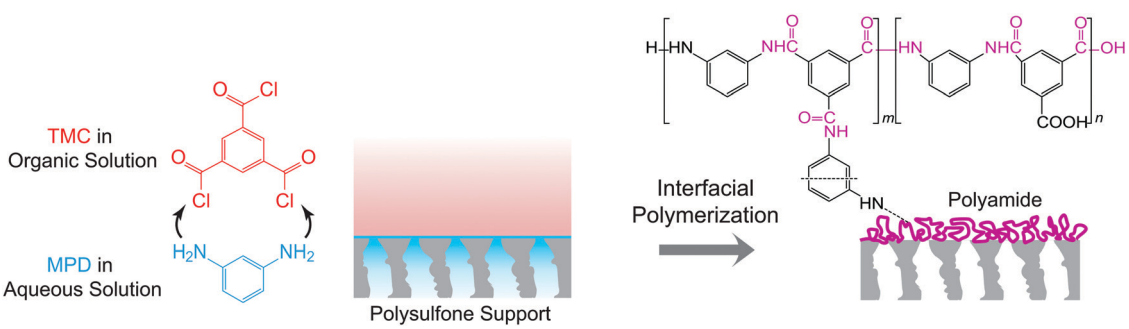

Fig. 3 Schematic representation of a typical interfacial polymerization process for making TFC RO membranes. The reaction between *m*-phenylenediamine (MPD) and trimesoyl chloride (TMC) occurs at the surface of a microporous polysulfone support to form a thin polyamide layer, whose chemical formula is illustrated. The *m* and *n* in the polymer structure represent the crosslinked and the linear segments, respectively ($m + n = 1$).

2. Current challenges in fabricating high-performance TFC membranes

2.1. Breaking the trade-off between permeability and selectivity

Mass transport in the dense, nonporous polyamide film of TFC membranes is governed by the solution-diffusion model. Water and solute molecules first partition into the polyamide layer, diffuse through the polymer matrix under chemical potential gradient, and desorb into the permeate side. Separation of fresh water from saline water is achieved because of the difference in the permeabilities of water and solutes in the polymer matrix. Water flux, J_w, is expressed as

$$J_w = A(\Delta P - \Delta\pi) \quad (1)$$

where A is the water permeability coefficient (or permeance), and ΔP and $\Delta\pi$ are the applied pressure and osmotic pressure differences across the active layer, respectively. Similarly, solute flux, J_s, is determined by

$$J_s = B\Delta C \quad (2)$$

where B is the solute permeability coefficient and ΔC is the concentration difference across the selective layer.

For a given membrane, the water and salt permeability coefficients of the active layer are determined by the intrinsic water permeability (P_w) and solute permeability (P_s), respectively:[9]

$$A = \frac{P_w V_w}{\delta_m R_g T} \quad (3)$$

$$B = \frac{P_s}{\delta_m} \quad (4)$$

where V_w is the molar volume of water, δ_m is the film thickness, R_g is the ideal gas constant, and T is the absolute temperature.

When plotting water–salt selectivity (P_w/P_s) *versus* water permeability (P_w) in Fig. 4A, performance data of existing TFC membranes are mostly confined in the blue-box region, wherein the highest selectivity for a given permeability approaches the solid line. This line represents the trade-off

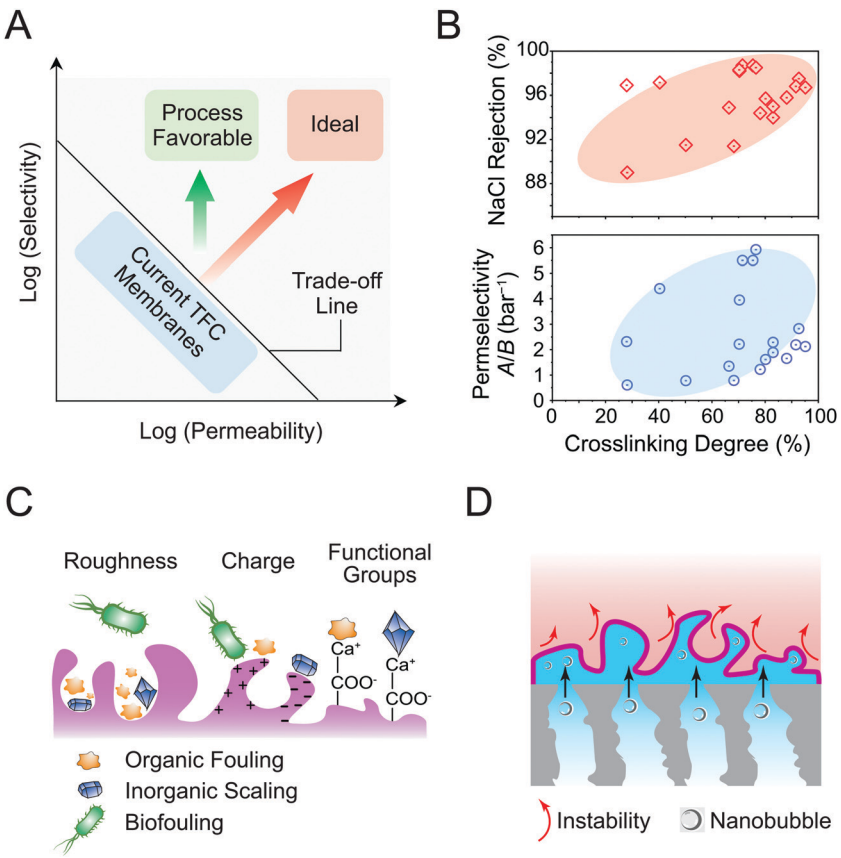

Fig. 4 Major challenges of interfacial polymerization and TFC membranes. (A) Permeability–selectivity trade-off relationship for TFC desalination membranes. Performance of current TFC membranes mostly lays in the blue box, in which the highest water–salt selectivity at a given water permeability is near the indicated trade-off line. Ideal membranes would have both high permeability and high selectivity, thereby breaking the trade-off relationship and laying in the top-right corner of the plot (red box). However, this combination is difficult to attain. A more practical strategy is to fabricate TFC membranes with comparable water permeability of current membranes but with increased water–salt selectivity (green box); this strategy can improve the efficiency of current desalination processes. (B) Correlation of crosslinking degree with salt rejection and permselectivity of TFC membranes. (C) Surface characteristics that determine fouling propensity of TFC membranes. (D) Proposed mechanisms for the origin of the characteristic ridge-and-valley structure of TFC membrane during interfacial polymerization: generation of interfacial instability in the organic phase and formation of nano-size bubbles in the aqueous phase.

relationship between permeability and selectivity, which is widely observed in membrane processes using synthetic polymer materials.[10] Ideal membranes should have high values of both water permeability and water–salt permselectivity (*i.e.*, the red-box region in Fig. 4A). Nevertheless, such a combination is difficult to achieve, as most material properties that affect water permeability would in turn exert similar effects on solute permeability. Indeed, the influence of material properties on salt permeability is more pronounced as salt permeability is proportional to the cube of water permeability ($P_s \propto P_w^3$).[9,11] That is, any increment in water permeability would lead to an exponential increase in salt permeability and thus a remarkable decrease in selectivity. Consequently, despite substantial efforts in optimization of IP reaction conditions, progress in pushing the trade-off line toward the ideal regime (*i.e.*, the red arrow in Fig. 4A) is relatively slow.

Instead of attaining membranes with high values of both water permeability and water–salt selectivity, recent studies emphasized the critical need for increased water–salt selectivity rather than increased permeability for the design of TFC membranes.[11,12] Based on process modeling of the desalination process, it was shown that further increments of water permeability would have marginal influence on the energy efficiency of RO systems. For example, in seawater desalination, a 5-fold increase of water permeance of existing TFC membranes would only lead to ~3.7% reduction in energy consumption.[11] Increasing water–salt selectivity is important because RO exhibits relatively poor rejection of small neutral molecules, such as boron and disinfection byproducts, thus necessitating post-treatment processes for their complete removal. These additional processes, in turn, lead to increased capital and operating costs, which could be avoided by using membranes with higher water–salt selectivity. Thus, increasing the water–salt selectivity of existing TFC membranes is a more effective strategy (the green arrow in Fig. 4A) for improving system efficiency and product water quality.

Water–solute selectivity of TFC membranes is determined by the combined mechanisms of steric hindrance, Donnan exclusion, and dielectric effect.[13] Steric hindrance is related to the pore size (or free volume) of polyamide, which allows molecules with smaller sizes to permeate while keeping larger ones from doing so. Donnan exclusion is governed by the fixed charge density on the membrane surface. For example, a negatively charged surface effectively rejects anions (*e.g.*, Cl^-). To maintain electroneutrality on both sides of the membranes, cations (*e.g.*, Na^+) are therefore also excluded by the membrane, leading to a good overall rejection of salts (*e.g.*, NaCl). The dielectric effect is related to an energetic penalty that solutes have to pay while transferring from a solvent with a high dielectric constant (*i.e.*, water) to a medium with a low dielectric constant (*i.e.*, polymer membrane material). The presence of such an energetic penalty thus hampers the diffusion of solutes (*e.g.*, salt ions) through the membrane.

The three solute rejection mechanisms discussed above are relevant to the material characteristics of the selective layer, which stems from the molecular structure of the polyamide materials. Taking crosslinking degree as an example, the polyamide forms a fully crosslinked structure (*i.e.*, the "*m*" segment in Fig. 3) with a monomer ratio of 3 : 2 for MPD to TMC. In an actual IP process, some linear segments (*i.e.*, the "*n*" segment in Fig. 3) would also form under a monomer ratio of 1 : 1 for MPD to TMC. In this case, unreacted acyl chloride groups undergo hydrolysis to form carboxylic groups, thereby imparting a negative charge to the membrane surface. The crosslinked segments more rigidly resist swelling due to the presence of chain linkages between polyamide backbones, thus impeding solute transport. In contrast, the linear segments are likely to undergo more severe swelling, which facilitates solute transport within the polymer matrix. As shown in Fig. 4B, both NaCl rejection and permselectivity exhibit an overall good correlation with the crosslinking density, *i.e.*, $m/(m + n)$, implying that increasing crosslinking segments is a feasible strategy toward the design of membrane with high water–salt selectivity. We note that this is only one example of how material characteristics determine membrane transport properties. Efforts to elucidate the structure–property–performance relationship of the polyamide selective layer will be of paramount importance in guiding the future design of high-performance TFC membranes.

2.2. Developing fouling-resistant membranes

Membrane materials effectively reject solutes to yield high-quality product water. During operation, the rejected solutes continuously accumulate on the membrane surface, leading to membrane fouling. Fouling is widely considered the Achilles heel for membrane processes as it leads to reduced process performance. For instance, the presence of a foulant layer increases the resistance for mass transport, resulting in a continuous decrease in water flux. Periodic physical or chemical cleaning is thus needed to mitigate fouling, leading to frequent system shutdown and increased operating cost. Therefore, understanding fouling mechanisms and developing effective antifouling strategies are of critical importance. Readers are referred to a recent comprehensive review to gain more insights into membrane fouling.[14]

In seawater desalination, membrane fouling can be classified into three categories (Fig. 4C): fouling by organic substances (*e.g.*, natural organic matter), scaling by inorganic species (*e.g.*, gypsum or silica), and biologic fouling by microorganisms (*e.g.*, bacteria or algae). The extent of fouling is governed by both membrane surface properties and feedwater solution chemistry. The surface properties of MPD-based TFC membranes—hydrophobic nature, roughness, and presence of carboxylic groups—are conducive to membrane fouling. Accordingly, surface modifications that render the membrane surface hydrophilic, smooth, and of neutral charge, have been widely proposed as effective antifouling strategies.[15,16] In addition to surface modification, fouling control could be achieved by adjusting solution chemistry prior to membrane desalination. For example, a large portion of organic and inorganic species could be removed in pretreatment processes by adding coagulants or adjusting pH, thereby reducing the overall fouling potential of the feedwater.[3]

Compared with other types of fouling, biofouling is even more challenging, owing to the growth and proliferation of

bacteria to form a sticky biofilm. Although the use of disinfectants (*e.g.*, chlorine) could effectively inactivate microorganisms, the chemical structure of polyamide is highly prone to degradation when exposed to oxidants like chlorine.[17,18] Polyamide degradation by chlorine undergoes a two-step reaction—N-chlorination and ring chlorination—resulting in irreversible damage to the polyamide selective layer and loss of salt rejection properties.[18] Therefore, complete removal of chlorine in the feedwater is needed before membrane filtration. Notably, after membrane filtration, the product water is often re-chlorinated for potable supply. Such complicated de- and re-chlorination procedures decrease system efficiency remarkably, thus necessitating the development of chlorine-resistant membranes for biofouling control.[17,18] Among the proposed strategies are the use of oxidation-resistant monomers, incorporation of sacrificial materials, or surface modification.[18,19] Despite these efforts, to date, there is no commercial chlorine-resistant desalination membrane, highlighting the challenges and the urgent need to develop such a membrane.

2.3. Understanding the reaction mechanisms of interfacial polymerization

Membrane desalination is an interfacial separation process where mass transport and fouling propensity are largely governed by membrane surface characteristics. To date, most surface characteristics (*e.g.*, wettability, charge, and functional groups) have been well investigated for their effects on membrane performance. Researchers have also developed numerous strategies to tune these characteristics for fabricating high-performance membranes. In contrast, the origin of membrane surface roughness resulting from the IP process and its role in membrane performance are relatively poorly understood.

The surface morphology of TFC membranes has a characteristic ridge-and-valley structure, with polyamide protrusions of ~100 nm. Such rough structure may shield accumulated foulants in the valley regions from being removed under the hydrodynamics of crossflow filtration, thereby leading to increased membrane fouling. In contrast, due to the presence of hollow cavities inside the protrusions, the rough morphology also increases the surface area for water transport, which is advantageous for TFC membrane design. As such, attaining surface morphology that could simultaneously inhibit fouling (low roughness) and facilitate water transport (high roughness) is challenging.

Precise control of surface morphology relies on understanding the formation mechanisms of the rough features during IP. Two mechanisms have been proposed for the formation of the ridge-and-valley structure during the IP process: interfacial instability and formation of nano-size bubbles. For interfacial instability, previous studies have suggested that the intense exothermic reaction between TMC and MPD increases the local temperature.[20] Such temperature change at the interface results in convective flow in the organic phase which forms the rough features (Fig. 4D, upper region). For the second mechanism—the formation of nanobubbles—studies suggest that the increased local temperature, together with the generation of byproduct hydrochloric acid in the TMD–MPD reaction, lead to the degassing of dissolved gas molecules (*e.g.*, CO_2, O_2, and N_2) in the aqueous phase (Fig. 4D, lower region).[21] These bubbles are then encapsulated by the nascent polyamide layer, leading to the formation of the ridge-and-valley structure. However, only indirect evidence was obtained for supporting these two mechanisms, thereby calling for more extensive efforts to reveal the mechanisms of roughness formation.

3. Emerging strategies of interfacial polymerization for fabricating TFC membranes

Recent advances in thin-film fabrication processes and material synthesis techniques enable innovative re-design of the IP process. These newly proposed IP strategies aim to endow TFC membranes with desired physicochemical characteristics, thereby leading to performance gains in fouling resistance or water–solute selectivity. Herein, we classify these emerging IP strategies into four categories according to their underlying design principles (Fig. 5) and discuss their respective advantages/disadvantages for making high-performance TFC membranes. Additionally, we compare the performance of membranes made using these emerging strategies to state-of-the-art commercial TFC membranes. Last, we discuss the key limitations of these IP strategies and general trends in the future development of IP.

3.1. Constructing sacrificial interlayers on the support layer

IP reaction is performed on a microporous support membrane that is formed by the non-solvent-induced phase separation (NIPS) process. In brief, a film of polymer dissolved in solvent is soaked in a non-solvent bath (*e.g.*, water or ethanol). The exchange of solvent and non-solvent leads to the precipitation of the dissolved polymer into a solid thin film, thereby producing a porous membrane structure.[22] However, as NIPS is largely a stochastic process, precise control over the structure of the microporous support is relatively challenging, necessitating more effective strategies for tuning characteristics of the support prior to IP.

One strategy that attracts a growing interest is to construct a sacrificial interlayer on the microporous support (Fig. 5A). The sacrificial interlayers are generally made from nanomaterials (*e.g.*, nanostrands, nanotubes, or metal–organic frameworks) with unique physicochemical properties (*e.g.*, shape, wettability, and charge), effectively modifying the support layer properties before IP. For example, a layer of needle-like cadmium hydroxide nanostrands was first deposited on a porous support.[20] Using the modified support for IP, the presence of this nanostrand layer moved the interfacial reaction away from the solid support, thereby resulting in a thin, smooth polyamide film.[20] Although this strategy was first demonstrated for membranes used in organic solvent separation,[20] similar techniques have recently been applied for membranes for seawater desalination.[23] Different from the nanostrand layer, researchers deposited a composite layer comprising a layer of carbon nanotubes (CNT) with a layer

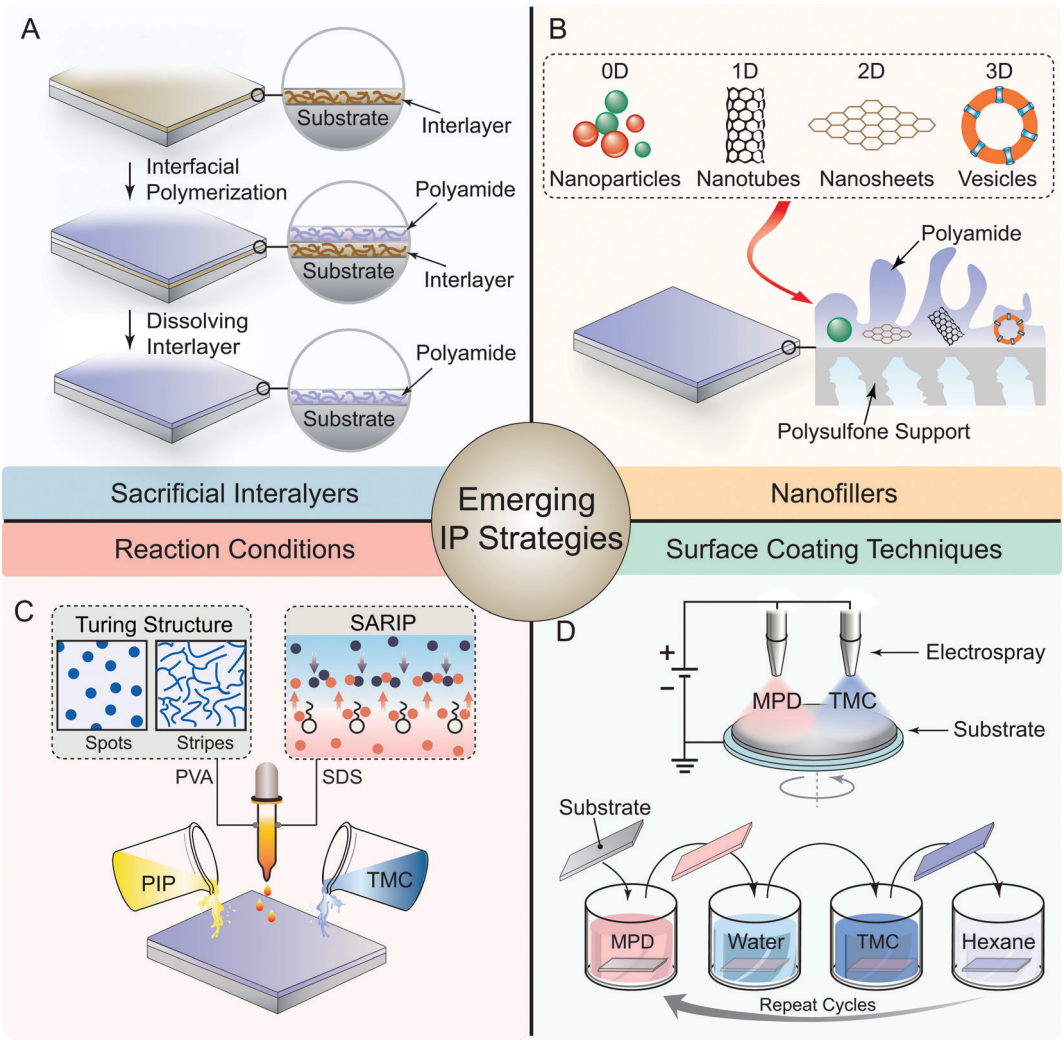

Fig. 5 Schematic diagrams of different types of emerging interfacial polymerization (IP) strategies for fabricating high-performance TFC membranes. (A) Use of sacrificial interlayers for tuning support layer properties prior to IP. A sacrificial layer is first deposited on a substrate (upper panel). IP is performed on the sacrificial-layer tailored substrate to form a polyamide layer on top (middle panel). The sacrificial layer is then removed by dissolving in a solvent (lower panel). (B) Embedding of nanomaterials into the polyamide layer for obtaining a mixed-matrix structure. Nanofillers include nanoparticles, nanotubes, nanosheets, and aquaporin vesicles, representing nanomaterials with 0D to 3D structures. (C) Tuning reaction conditions of IP by adding different additives. In the upper left panel, the addition of polyvinyl alcohol (PVA) to the aqueous phase reduces the diffusion rate of PIP, leading to a diffusion-driven instability and generating nanoscale spotted and striped Turing structures. In surfactant assembly regulated interfacial polymerization (SARIP) (upper right panel), the addition of a surfactant, sodium dodecyl sulfate (SDS), results in a self-assembled network of amphiphiles at the water/hexane interface, which facilitates the transport of PIP (red dots) across the interface to react with TMC (black dots). (D) Incorporation of new surface coating techniques into IP processes. In electrospray process (upper panel), MPD (in aqueous phase) and TMC (in organic phase) solutions are respectively introduced to two separate nozzles. A substrate stage is grounded and connected to the two nozzles with a direct current power source. When high voltage is applied, the charged liquids leave the needles and emit microdroplets to deposit onto the substrate, where the reaction between MPD and TMC leads to the formation of a thin polyamide film. In the molecular layer-by-layer process (lower panel), a substrate is alternately dipped into the two monomer solutions (*e.g.*, MPD in water and TMC in hexane) and subsequently rinsed with proper solvents (water and hexane) after each dipping step. Such a dip-coating process is repeated for several cycles, resulting in a thin, defect-free film comprising multilayers of polyamide.

of zeolitic imidazolate framework (ZIF-8) on top.[23] After the IP reaction, the embedded ZIF-8 could be dissolved by immersing the membrane in water, leading to the formation of a hollow polyamide layer with crumpled surface structure. Such crumpled structure resulted in an enhanced water permeability without compromising salt rejection properties. Readers are referred to a comprehensive review for the recent progress in the use of sacrificial interlayers in IP.[24]

In addition to the use of nanomaterial-tailored supports, another strategy is to perform IP at a free interface between an aqueous phase and an organic phase.[25,26] The liquid interface enables more rapid heat dissipation than that in an aqueous solution trapped in solid support, forming free-standing nanofilms with smooth surfaces due to inhibition of interfacial instability. The formed film could be used directly or transferred to another porous support for performance

evaluation. Such a strategy provides a useful platform for isolating polyamide layers for advanced characterization in order to unravel the structure–property–performance relationship of the polyamide selective layer. However, as the polyamide layer is relatively fragile with low mechanical strength, integrating such free-standing films into membrane modules will be extremely challenging. Moreover, even with an underlying support, the interaction between the polyamide and the support will be much weaker compared with that of conventional TFC membranes. Such low interaction would result in low resistance of the polyamide films to high-pressure or high-crossflow conditions, causing the films to lose their integrity during operation. Therefore, further advances in material and process designs are needed for expanding the real-world application of these free-standing polyamide membranes.

3.2. Embedding nanofillers in the polyamide active layer

Embedding fillers in the polyamide selective layer is, potentially, a direct strategy toward high-performance TFC membrane fabrication (Fig. 5B); this strategy has been a topic of interest for more than two decades.[27] Following a typical IP process, pre-synthesized fillers are added to the organic phase (mixed with TMC) or aqueous phase (mixed with MPD), forming a mix-matrix structure in the resulting polyamide layer. Early efforts largely focused on the use of different nanofillers (*e.g.*, nanoparticles, nanotubes, and nanosheets), which endowed the polyamide layer with favorable properties such as high water permeance and biofouling resistance. These attempts have introduced the concept of thin-film nanocomposite (TFN) membranes; readers are referred to a comprehensive review to learn more about TFN membranes.[27] In the past decade, other emerging materials with desired characteristics have also been considered as embedded blocks in the polyamide layer. For example, researchers prepared lipid vesicles laden with aquaporins, which have unique water channels with high water permeability and salt selectivity.[28,29] The presence of the aquaporin water channels facilitated water transport through the polyamide layer while retaining ionic species, and readers are referred to a recent comprehensive review.[30]

Despite the reported performance gain in water permeance and fouling resistance through adding filler materials, real-world applications of such composite membranes are still hindered by several challenges, casting doubt about their potential applicability. The most critical factor is the inevitable formation of defects at the interface between fillers and the polyamide matrix, which has been a long-standing issue for all types of dense membranes with a mixed-matrix structure.[31] The formation of these defects is either ascribed to the low miscibility between the two materials, or the inhibition of the IP reaction to form less crosslinked polyamide regions. For example, a recent study has observed the presence of non-selective defect channels with a size of ~2 nm between

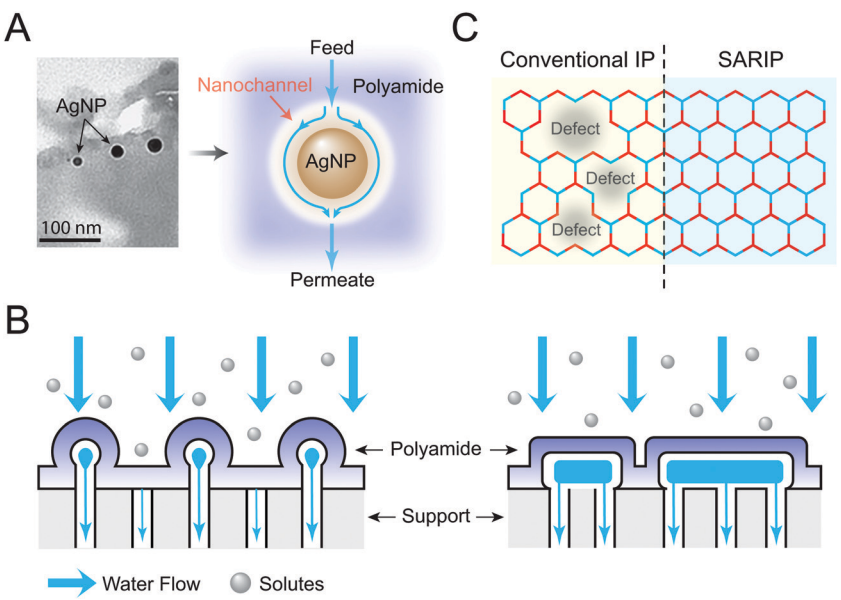

Fig. 6 Characteristics and performance of TFC membranes fabricated through emerging interfacial polymerization (IP) strategies. (A) Effect of embedded nanofillers on the mass transport of TFC membranes. Cross-section image of a polyamide layer with embedded silver nanoparticles (AgNP) (left panel). The light-colored haloes around the silver nanoparticles correspond to lower mass density, suggesting the possible formation of nanochannels with a size of 2–3 nm between a silver nanoparticle and the polyamide matrix (right panel). These channels potentially facilitate water permeability while compromising water–solute selectivity. Scanning electron microscopy is adapted with permission from ref. 32, American Chemical Society. (B) Schematic illustration of spatial distribution of water permeability sites with different polyamide morphologies, including spotted (left panel) and stripped (right panel) Turing structures. Figure is reproduced with permission from ref. 39, American Association for the Advancement of Science. (C) Schematic illustrations of a polyamide selective layer formed *via* conventional IP (left), which has a heterogeneous pore size distribution with the presence of large pores, and surfactant-assembly regulated IP (SARIP) (right), which has a uniform pore size distribution. The uniform pore structure endows the SARIP membranes with a precise solute–solute separation.

embedded silver nanoparticles and polyamide matrix (Fig. 6A),[32] which are detrimental to membrane water–salt selectivity. Although modifying fillers with hydrophobic materials may enhance their miscibility in the polyamide matrix and thus inhibit the formation of the defect channels,[33] the high liquid entry pressure (LEP) in these hydrophobic nanopores would provide additional resistance to water transport.[34] For instance, a hydrophobic mesoporous material (contact angle of 140°) with a pore diameter of 4 nm requires an LEP of 138 bar, which is beyond the maximum operating pressure in typical RO systems (*i.e.*, ~80 bar). Notably, the use of the fillers in desalination membranes may also result in the release of some filler materials to the product water, leading to human exposure to these materials and potential health impacts.[1]

3.3. Tuning reaction conditions of interfacial polymerization

Tuning reaction conditions of IP has been widely researched since the origin of the TFC membranes. Previous efforts through the control of monomer concentrations or adjustment of curing conditions of IP have resulted in numerous commercial products.[8,35] New strategies involve the use of new reaction monomers and additives in IP for making high-performance TFC membranes.

Conventional IP is performed between a triacyl chloride (particularly TMC) with a diamine—typically MPD for RO, and piperazine (PIP) for NF. The reaction utilizes the high reactivity between acyl chloride and amine groups, thereby readily forming a dense selective layer at the organic–aqueous solution interface. In essence, any pair of reactive chemicals, which can be respectively dissolved in organic and aqueous phases, could be potential monomers for IP. For example, recent studies reported the use of hydroxyl-rich cyclodextrins as alternative monomers of diamine to react with TMC.[36] The porous cyclodextrin molecules endow the formed nanofilms with unique Janus pathways (*i.e.*, hydrophobic inner cavities and hydrophilic channels), thereby enabling precise molecular sieving in both organic solvent separation and desalination. Notably, recent efforts have expanded the search of alternative monomers for IP to a broader range of chemicals as described in these comprehensive reviews.[37,38]

Besides the use of new monomers, progress has also been made in adding various additives to the IP reaction (Fig. 5C).[39,40] Different from new monomers, these additives do not become segments of the resulting polyamide polymer. Instead, they influence the formed polyamide selective layer by inhibiting or facilitating the reaction between acyl chloride and diamine at the interface. For example, in the conventional IP process, the reaction predominantly occurs on the organic side (*i.e.*, TMC solution) of the interface, owing to the high diffusivity of diamine monomers (*e.g.*, MPD or PIP) from the aqueous phase to the organic phase. Adding a macromolecule—polyvinyl alcohol (PVA)—to the aqueous phase effectively inhibits the diffusion of PIP, thus leading to a diffusion-driven Turing instability at the interface (Fig. 5C, upper left panel).[39] By adjusting the amount of the PVA additive, the surface morphology of the polyamide layer could be manipulated to form spotted (Fig. 6B, left panel) and striped (Fig. 6B, right panel) Turing structures, thereby affecting the water transport in the resulting membranes. In another study,[40] an opposite strategy was proposed to enhance the diffusion of PIP by adding surfactant additives to the aqueous phase of diamine, leading to a new IP process—surfactant assembly regulated interfacial polymerization (SARIP) (Fig. 5C, upper right panel).[40] It was suggested that the trans-interface diffusion of PIP in the conventional IP is a rate-limiting step, resulting in a heterogeneous polyamide network (Fig. 6C, left panel) with a broad distribution of pore sizes. Addition of sodium dodecyl sulfate (SDS) molecules to the aqueous phase in SARIP leads to the formation of a self-assembled dynamic network that facilitates the diffusion of PIP across the interface. The increased amount of PIP in the TMC solution results in a more homogeneous IP reaction, thus forming a polyamide network with a more uniform pore size distribution (Fig. 6C, right panel). Consequently, the SARIP membrane exhibited a sharper cut-off for ion separation than the conventional IP membrane, potentially enabling precise separation in desalination and water purification.

3.4. Incorporating emerging surface coating techniques into interfacial polymerization

The above-mentioned strategies involve the use of new chemicals (*e.g.*, nanostrands, nanofillers, monomers, or additives) for tailoring the IP process. Presently, polyamide chemistry made from MPD and TMC monomers remains the gold standard for commercial RO membranes. This fact has driven innovations in the manufacturing process of IP (Fig. 5D), while retaining the use of the conventional MPD–TMC monomers—the pair that shows relevance and potential to the industrial fabrication process.

As discussed above, the trans-interface diffusion of MPD molecules is the major factor limiting the homogeneous formation of a polyamide network. Additionally, the fast kinetics of the MPD–TMC reaction lead to rapid formation of a polyamide network, as the solution at the interface readily reaches the gel point. This nascent polyamide gel provides additional resistance for the diffusion of the two monomers during the reaction. Consequently, the conventional IP process produces selective polyamide layers with strong depth heterogeneity (*i.e.*, variation in chemical structure from the surface to the bottom) and rough surface morphology (*i.e.*, characteristic ridge-and-valley structure).[41] To overcome these limitations, molecular layer-by-layer (mLbL) deposition was proposed as an alternative IP process (Fig. 5D, lower panel).[42] In this technique, a pretreated substrate is sequentially immersed in MPD and TMC; the immersion is repeated for several cycles to obtain an integral polyamide film. Notably, after each soaking, the substrate is thoroughly rinsed to leave only a thin layer of the reaction solution on the surface. In this case, the mLbL technique builds the film with one molecular layer at a time *via* instantaneous reaction of alternating MPD/TMC monomers, thereby facilitating complete reaction between the monomers to form an integral polyamide network. Compared with membranes made through conventional IP, the mLbL-polyamide film not only

has a smooth surface with enhanced fouling resistance, but also exhibits increased NaCl rejection.[42] Moreover, the mLbL technique enables fine-tuning of reaction conditions (*e.g.*, monomer/solvent type, concentration, and support materials), as well as nanoscale control of thickness, topology, and local chemical composition of resulting polyamide films. Hence, the mLbL technique holds promise as a versatile platform for revealing the reaction mechanisms of IP.

Compared with the mLbL technique, more precise control of reaction conditions could be achieved by integrating an electrospray technique—an ionization method developed for mass spectroscopic analysis of polar biomolecules[43]—to the IP process.[44,45] In this process, MPD and TMC monomer solutions are respectively loaded into two syringes (Fig. 5D, upper panel). After applying a high voltage to the solution, the charged solutions are ejected from the metallic needle and burst into fine sprays due to the repulsive Coulombic forces. When both MPD and TMC sprays deposit on a substrate, the polymerization reaction takes place to form a polyamide layer. In essence, the dropwise deposition of monomer solutions confines the MPD–TMC reaction to the interface of the microdroplets, leading to the formation of a smooth polyamide film.[44,45] This process enables nanoscale control of the film thickness ($\sim$4 nm) through simple manipulation of reaction conditions, such as monomer concentration,[44] spraying time,[45] or use of different supports.[44] Notably, the formed polyamide film exhibits a thin layer ($\sim$10 nm) and good NaCl rejection (>95%),[44] demonstrating the promise of this emerging IP process in making a thin, defect-free polyamide film for desalination.

3.5. Performance summary of TFC membranes made through emerging techniques

As discussed earlier in this Tutorial, TFC membranes are constrained by the permeability–selectivity trade-off (Fig. 7). The intrinsic properties of commercial TFC membranes made by conventional IP (blue squares) lay beneath an upper-bound line. Such a trade-off relationship also holds true for TFC membranes fabricated through emerging IP strategies (red circles). Although the two groups of membranes exhibit comparable water permeability values in the range of 1 to 5 L m^{-2} h^{-1} bar^{-1}, the conventional-IP membranes substantially outperform the emerging-IP membranes in water–salt selectivity. Such results are not surprising, as the commercial membranes are the products obtained after a long-term optimization process. Presently, emerging IP strategies are still at the stage of lab-scale research, involving hand-cast procedures in making membranes. We expect that some performance enhancement of the emerging-IP membranes could be achieved by employing standard manufacturing processes. However, the potential and feasibility in scaling up these emerging IP strategies into real-world industrial production processes should be carefully considered and evaluated.

Notably, the low permselectivity of the emerging TFC membranes was largely ascribed to the poor rejection of NaCl salt. For instance, based on projected NaCl rejection,[46] the area beneath the upper bound line could be divided into several regions targeting different applications (Fig. 7, shaded areas). The commercial membranes with excellent rejection of NaCl largely lay in the seawater desalination RO region (SWRO, grey area, R_{NaCl} > 99%), while the majority of the emerging TFC membranes are in the brackish water RO region (BWRO, yellow area, 99% > R_{NaCl} > 90%,) or nanofiltration region (NF, blue area, R_{NaCl} < 90%). As seawater is the dominant feedwater source in the global share of desalination for water production (>60%),[6] substantial efforts are needed to improve the water–salt selectivity of the emerging TFC membranes, thereby improving their performance for SWRO uses.

Notably, despite the performance gap between commercial and emerging TFC membranes made of the polyamide chemistries, the latter largely outperform membranes made of new emerging materials, such as nanotubes and nanosheets (purple hexagons), in terms of water–salt selectivity. While the discussion on

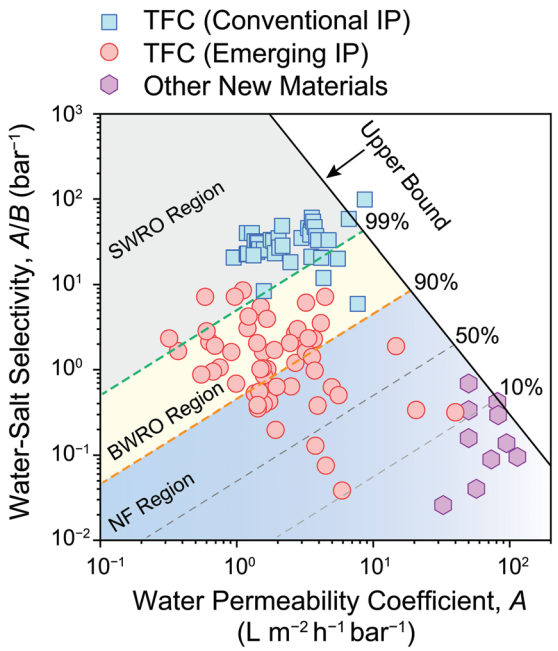

Fig. 7 Water permeability and water–salt selectivity of different types of desalination membranes. The blue squares represent the performance of commercial TFC membranes made through conventional IP. These values are adapted from ref. 22. The red circles represent lab-made TFC membranes fabricated *via* some emerging IP strategies reviewed in this Tutorial. The transport properties of some emerging membrane materials are also included in the figure for comparison (purple hexagons). The green and orange dashed lines correspond to NaCl rejections of 99% and 90%, respectively, at a water flux of 20 L m^{-2} h^{-1}. The area under the upper bound line is further divided into three regions based on the threshold NaCl rejection of 99% and 90%. Most commercial TFC membranes have rejections in the seawater reverse osmosis (SWRO) region (rejection > 99%), while the emerging TFC membranes have rejections in the brackish water reverse osmosis (BWRO) region (90% < rejection < 99%) and the nanofiltration (NF) rejection (rejection < 90%). The separation performance of the conventional TFC membranes is relatively closer to the upper bound line, owing to the well-developed and optimized systems for the conventional IP. In contrast, the data points of the emerging TFC membranes are far below the upper bound line, suggesting that substantial efforts are needed to further optimize the fabrication conditions of the emerging IP strategies.

desalination membranes made from emerging materials *via* non-IP methods is beyond the scope of this Tutorial, the low performance of such membranes has been attributed to defects inherent in the top-down fabrication methods used.[22] Nevertheless, our analyses above demonstrate the promise of the polyamide chemistries as well as the IP-based processes for making high-performance desalination membranes.

4. Emerging techniques in characterization of TFC membranes

Insights gained through in-depth characterization of TFC membranes are important not only for understanding the structure–property–performance relationship, but also for future design and optimization of IP-based processes. Previous efforts in probing TFC membrane structures largely relied on the use of conventional tools, such as spectroscopy [*e.g.*, X-ray photoelectron spectroscopy (XPS) and Fourier-transform infrared (FITR) spectroscopy] and microscopy [*e.g.*, scanning electron microscopy (SEM), transmission electron microscopy (TEM), and atomic Force Microscope (AFM)] techniques.[47] These tools have provided general structural information about TFC membranes, like ridge-and-valley morphology, degree of crosslinking, and functional group distribution of the polyamide layer, facilitating the understanding of the TFC membranes.

As discussed above, IP is a rapid self-inhibiting process that enables the formation of a thin, defect-free polyamide film. These features of IP, in turn, pose challenges for nanoscale characterization of TFC membranes. For instance, when exploring IP reaction mechanisms, the fast reaction kinetics between amine and acyl chloride limit the direct observation of polyamide network formation during the IP reaction using conventional characterization tools. Moreover, the formed thin polyamide film ($\sim$100 nm) only accounts for $\sim$1‰ of the total thickness of a typical TFC membrane ($\sim$100 μm for the underlying polysulfone support and PET fabric layers). When characterizing the polyamide layer *via* conventional spectroscopic techniques, the underlying support materials generate substantial amounts of background noise that interferes with the characteristic information of polyamide, hampering a closer look at the polyamide layer alone. Consequently, along with the progress in developing emerging IP strategies, recent years have also witnessed substantial efforts in exploring new techniques for TFC membrane characterization. These newly developed techniques could be classified into two categories: direct imaging techniques and indirect non-imaging techniques. An overview of these techniques is presented below, and the pros and cons of each technique are reviewed and discussed.

4.1. Direct imaging techniques

Direct imaging techniques aim to provide visual structural information of the polyamide layer by using electron microscopic tools (Fig. 8). In a regular cross-section TEM image (Fig. 8a$_1$), a characteristic ridge-and-valley structure could be observed on the top surface of TFC membranes. However, discerning the polyamide–polysulfone interface (*i.e.*, the boundary between active and support layers) in such dark-field images is difficult, because the polymeric materials with dominant light elements (*e.g.*, C, H, and O) on their backbones are nearly "transparent" to electrons. Such a technological gap necessitates effective measures to enhance the contrast difference (Fig. 8A), thereby illustrating fine structures of the polyamide layer and the polyamide–polysulfone interface.

One simple strategy is to stain the polyamide layer with heavy metal elements (such as osmium, ruthenium, uranyl, and lead).[48–50] In a general procedure, TFC membranes are immersed into a metal oxide solution, in which metal ions readily approach and adhere to the charged regions of the polyamide film. The stained membranes then undergo identical sample preparation processes (*i.e.*, fixation, dehydration, and sectioning) and are imaged using electron microscopic techniques. The metal stains absorb electrons or scatter part of the electron beam which otherwise is projected onto the sample. As a result, the stained polyamide layer is brighter than the unstained polysulfone support in the dark-field images (Fig. 8a$_2$). Previous studies utilized such enhanced contrast to map the distribution of functional groups in the polyamide layer.[48,49] Recent efforts—through tailoring staining conditions, together with advances in a high-resolution electron microscope—have enabled a closer look at the inner structure of the polyamide layer.[50] For example, precipitation of the metal stains on the outer surface of the polyamide clearly illustrates the nodular shape of the polyamide (Fig. 8a$_2$). Moreover, the distribution of aqueous stain tracers reflects actual transport pathways in the polyamide layer, thereby revealing the "channel" structure for water transport within the polyamide layer (inset of Fig. 8a$_2$).[50] Although such "channels" were also observed in non-stained samples (white arrows in Fig. 8a$_1$), staining substantially enhanced the contrast for visualizing such fine structures.

Elemental mapping is another strategy for enhancing interfacial contrast.[41] In particular, the polyamide active layer is rich in nitrogen while the underlying polysulfone support layer contains sulfur but no nitrogen. This intrinsic elemental contrast allows researchers to perform an analysis using scanning transmission electron microscopy (STEM) coupled with energy-dispersive X-ray spectroscopy (EDX), for elucidating the nanoscale structure and chemical composition.[41] In the mapping image (Fig. 8a$_3$), fine structures at the polyamide–polysulfone interface could be observed. For example, the presence of cavities inside the ridge structure of both membranes (white arrows) suggests depth heterogenicity of the polyamide film. Additionally, the polyamide layer comprises a continuous 50 nm-thick polyamide base layer (yellow arrow and bracket), from which the ridge-and-valley structure extends outward.

Direct imaging of polyamide internal microstructure could also be achieved through the isolation of the polyamide layer, followed by 3D tomography visualization (Fig. 8B).[51] In the isolation step, the TFC membrane is immersed in a polar solvent (*e.g.*, DMF, NMP, and THF) to dissolve the underlying polysulfone layer, while the structure of the insoluble

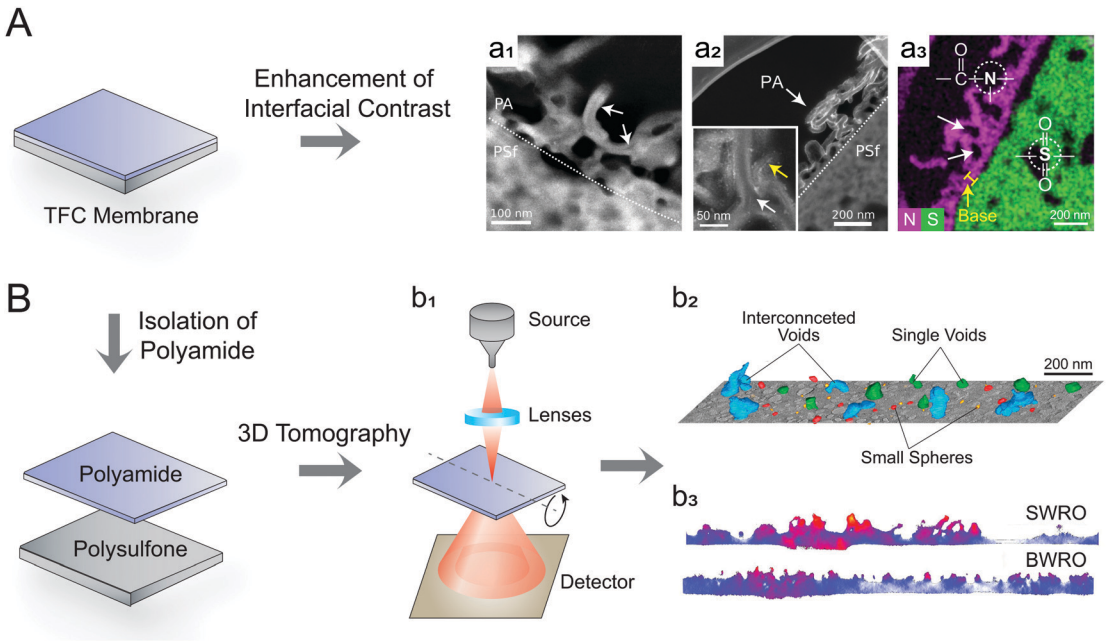

Fig. 8 Direct imaging techniques for the characterization of TFC membranes. (A) Enhancement of interfacial contrast for the direct visualization of polyamide–polysulfone interfacial structure. Comparison of scanning transmission electron microscopy (STEM) cross-section images of a non-stained (a_1) and a stained (a_2) TFC membrane. Metal stains bound to the polyamide active layer result in convoluted regions (white arrowhead), enabling differentiation of the interface and observation of the polyamide internal structure. The inset shows higher magnification of a region of polyamide layer with empty (white arrow) and filled (yellow arrow) channels. Scanning electron microscopy images are adapted with permission from ref. 50, Elsevier. (a_3) Elemental mapping also presents a clear interfacial structure of a TFC membrane. This technique utilizes the elemental contrast between the polyamide (abundant in nitrogen) and polysulfone (abundant in sulfur) layers. "N" (magenta) denotes nitrogen and "S" (green) denotes sulfur; the white arrows indicate the cavities inside the ridge structure, while the yellow arrow and bracket indicate the dense polyamide layer. Scanning electron microscopy image is adapted with permission from ref. 41, American Chemical Society. (B) Isolation of the polyamide layer for 3D tomographic characterization. (b_1) Schematic illustration of tomography techniques. A range of 2D images are collected using an advanced electron microscope by tilting the polyamide film sample to many different angles. The 3D structure of the sample is then reconstructed from the images, thereby enabling further analysis of its structural characteristics. (b_2) 3D visualization of the spatial distribution of pore structure of various sizes within the interior of a polyamide film isolated from a commercial TFC membrane. The pores are classified based on their respective internal sizes: singe voids have a size larger than 30 nm (green) while the spheres have a size smaller than 30 nm (red) or 15 nm (yellow). Some single voids are connected to form some giant pores (blue). Figure is adapted with permission from ref. 51, Elsevier. (b_3) Tomographs of two commercial TFC membranes for SWRO and BWRO applications. The intensity of the polyamide layers is displayed as a heat map, where red corresponds to higher intensity. Figure is adapted with permission from ref. 52, United States National Academy of Sciences.

polyamide network is largely retained. The isolated polyamide film is then imaged by TEM 3D tomography. By rotating the sample around the tilt axis, a series of 2D projection images are acquired at different tilt angles (normally within a range of -79° to $+79^\circ$). After alignment and processing, the tilt series are reconstructed into a 3D model of the isolated polyamide film, thereby providing information on its internal structure.[51] For example, in a tomogram of a commercial TFC membrane (Fig. 8b_2), internal voids with various sizes and shapes were clearly illustrated.[51] These voids, which govern the pathways of flow and diffusion across the polyamide layer, were either connected to the outside of the polyamide film or encapsulated within the polyamide matrix.

Following the progress in TEM tomography, scanning TEM (STEM) has also been introduced for imaging polyamide layers (Fig. 8b_1).[52,53] Unlike the use of a parallel, coherent beam of electrons for imaging in conventional TEM, STEM technique scans a focused beam of electrons across a sample. Such dynamic focus effectively reduces the defocus variation in TEM imaging of a thick sample at a high-tilt angle,[52] thereby providing high-quality images of soft materials for nanoscale analysis. Moreover, STEM tomography operated in high-angle annular dark-field (HAADF) mode can provide additional information about polymeric structures, such as mass, thickness, and atomic number.[52,53] For instance, in heat maps of the STEM images of two commercial TFC membranes (Fig. 8b_3), the membrane for seawater RO (SWRO, upper panel) exhibits a much denser structure (red area) than that of the membrane for brackish water RO (BWRO, lower panel).[52] The denser structure is likely the actual selective barrier of polyamide, which is responsible for the higher salt rejection and lower water permeance of the SWRO membrane compared to the BWRO.[52,53]

4.2. Indirect non-imaging techniques

Parallel to efforts in direct imaging techniques, progress has also been made in using non-imaging techniques for TFC membrane characterization. These techniques, coupled with spectroscopic or scattering tools, shed light on chemical composition, nanopore size distribution, and polymeric chain

structure within the polyamide layer, thereby providing additional valuable information for revealing the membrane's internal structure.

As discussed earlier, conventional spectroscopic methods provide limited information about the polyamide internal structure. Researchers sought to develop effective characterization strategies to fully explore the capability of the spectroscopic techniques. An earlier example was impregnating the polyamide layer with silver nitrate solution, in which silver ions selectively bind to negatively charged carboxyl groups at a 1:1 ratio.[54] The impregnated polyamide is then characterized by Rutherford backscattering spectrometry (RBS), which detects the amount of the bound silver probe for determining the volume density of carboxyl groups. Using this technique, other useful information, such as ionization behaviors and ion accessibility, could also be revealed by adjusting characterization conditions (*e.g.*, impregnation pH or ion probe types).[54] However, this silver-RBS method has not been widely used in membrane characterization, largely owing to the inaccessibility of the specialized RBS instrument. In a later effort,[55] researchers modified the silver-binding procedure used in RBS by including a low-pH elution step, which allowed the use of a more accessible spectroscopic technique—inductively coupled plasma mass spectrometry—to quantify the eluted silver concentration for determining carboxyl density of the polyamide layer.

In addition to the volume density of functional groups, spectroscopic techniques could also be combined with incident high beams for revealing the depth profile of the polyamide layer.[41,56] For example, XPS—a technique that only probes the very top surface of the polyamide layer (<5 nm)—could be paired with C_{60}^+ cluster ion sputtering platform.[41] In this combined technique, the polyamide side of TFC membranes is exposed to a high beam generated from C_{60}^+ bombardment, enabling controllable sputtering of the polyamide layer. At different sputtering times, XPS elemental scans are performed on the sputtered spot in order to reveal the atomic composition and chemical state of the organic thin films with depth.[41] In a similar technique called elastic recoil detection (ERD), a membrane sample is bombarded with a high-energy iodine beam, causing target atoms (*e.g.*, C, N, O, S, and Cl) to be scattered out of the sample.[56] Analysis of the scattered signal not only identifies the recoil ion species according to their respective nuclear charge or mass, but also detects the energy of the recoil ions.[56] This latter information is then used to determine the energy loss between the projectile and the recoil ion within the sample matrix, thereby enabling analysis of elemental depth profiling of the membrane sample. Notably, the depth profiles extracted from these spectroscopic tools (*i.e.*, XPS-C_{60}^+ and ERD) revealed the presence of a heterogeneous layer that contains both polyamide and polysulfone signatures.[41,56] Such a structure implies that the polyamide penetrates the pores of polysulfone during IP reaction, anchoring to the support to form a stable TFC structure.

Positron annihilation lifetime spectroscopy (PALS) is another technique capable of probing the internal pore structure of the polyamide layer on TFC membranes.[57] The analysis is conducted by injecting low-energy positrons into the polyamide layer, where each positron combines with an electron to form an electron–positronium (Ps) ion. These Ps ions tend to locate in electron-deficient regions, such as free volume and pores, and undergo a slow self-annihilation process with a long lifetime. In electron-rich regions that were occupied by the polyamide matrix, the Ps ions would interact with surrounding molecularly bound electrons to induce a rapid annihilation process with a short lifetime. By correlating the lifetime of the injected positrons with the sample void size, PALS could reveal characteristics of pore structure, such as size, distribution, and film thickness. For example, using this technique, researchers were able to reveal the presence of two types of pores within the polyamide layer of an RO membrane, *i.e.*, smaller intrachain network pores (~0.45 nm) and larger interchain aggregate pores (~0.8 nm).[57] This sub-nanometer insight has enabled substantial progress in elucidating the structure–performance relationship of TFC membranes, as well as in understanding the reaction mechanisms on IP. Readers are referred to a recent comprehensive review for a detailed introduction of PALS in membrane characterization.[58]

Besides advances in spectroscopic techniques, recent years have also witnessed increasing interest in using scattering techniques for TFC membrane characterization (Fig. 9).[59–61] During the measurements, the incident sources (*e.g.*, X-ray or neutron) are scattered by the electrons (X-ray) or the nuclei (neutron) to generate corresponding signals (Fig. 9A). Generally, the interference of scattered sources from neighboring planes could be described by Bragg's law: $n\lambda = 2d\sin\theta$, where θ is the scattering angle, d is the distance between the atomic planes (d-spacing), λ is the wavelength of the incident source, and n is an integer. As the scattering vector, q, is related to θ by the relation $q = 4\pi\sin\theta/\lambda$, Bragg's law could be written as $d = 2\pi/q$. In principle, Bragg's law is applicable to crystalline materials with repeating discrete reflections. However, the inverse relationship of the actual length scale, d, and the reciprocal space, q, could still be used in the interpretation of the interchain distance in amorphous materials, such as highly crosslinked polyamide. For example, wide-angle X-ray scattering (WAXS) generally collects scattered signals with $q > 0.5$ Å^{-1}, corresponding to the atomic or molecular structures with $d = 0.1$–10 Å, while small-angle X-ray scattering (SAXS) or small-angle neutron scattering (SANS) collect scattered signals with q range of 0.005–0.5 Å^{-1} for revealing mesoscale structure (*i.e.*, d = 10–1000 Å) from the aggregates or clusters of atoms and molecules.

Two types of polyamide samples are commonly used in scattering experiments: polyamide film and bulk dispersion. In film characterization mode (Fig. 9B), incident X-ray is shed on a polyamide film at a relatively small angle, and scattered signals are then detected by a 2D detector.[59] As the film is horizontally positioned on a sample stage, analysis of scattering patterns could provide information on both molecular structure and preferential orientation (either in-plane or out-of-plane) of the polyamide network.[59] For example, an arc-like meridional scattering feature in a WAXS pattern (Fig. 9C), where intense scattering is preferentially aligned along the vertical q_z direction, implies the in-plane orientation of aromatic stacking in the

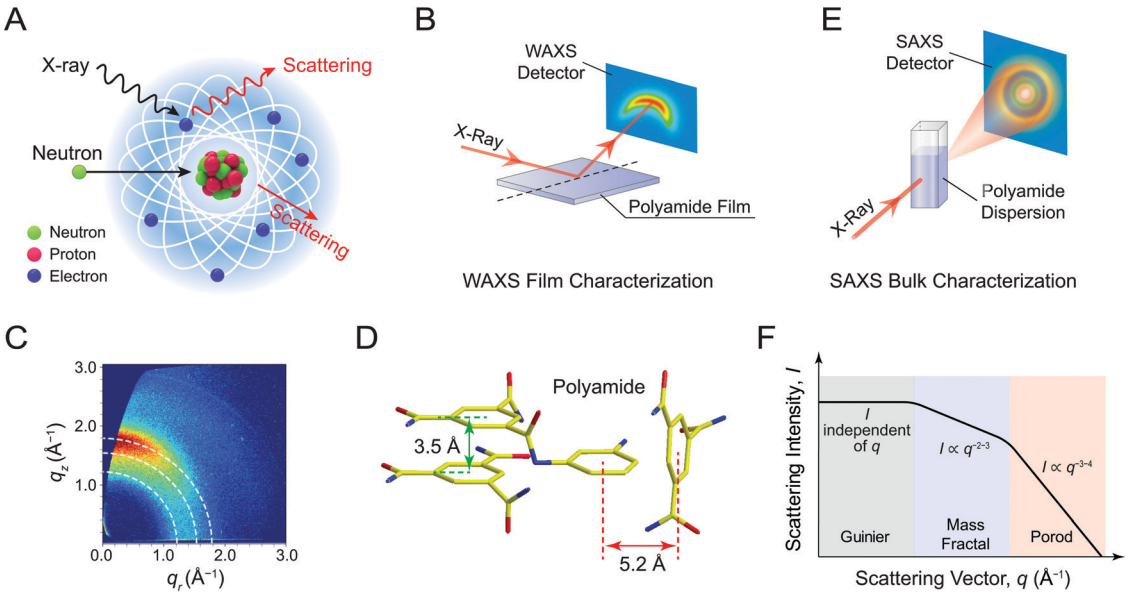

Fig. 9 Indirect scattering techniques for the characterization of TFC membranes. (A) Interaction of atomic matter with scattering sources to generate scattering signals. X-rays interact with electrons in the material *via* an electromagnetic force, while neutrons interact with the nucleus *via* the very short-range strong nuclear force. (B) Schematic illustration of the experimental setup used for characterizing a polyamide film using wide-angle X-ray scattering (WAXS). A representative anisotropic pattern on a 2D WAXS detector provides information on the molecular structure and preferential orientations in the polyamide film. (C) A representative WAXS pattern of a polyamide film. The horizontal (q_r) and vertical (q_z) vectors correspond to the surface parallel and normal scattering wave vectors, respectively. Dashed arcs are scattering vectors of 1.22, 1.54, and 1.79 Å^{-1}, corresponding to the spacing of 5.2, 4.1, and 3.5 Å, respectively. Figure is adapted with permission from ref. 59, American Chemical Society. (D) Different stacking behaviors of aromatic rings within a polyamide layer. The green dashed lines indicate the distance of 3.5 Å for the aromatic cores stacked in π–π (parallel) structure, while the red dash lines indicate the distance of 5.2 Å for the aromatic cores stacked in T-shaped (orthogonal) structure. (E) Schematic illustration of small-angle X-ray scattering (SAXS) platform used for characterizing polyamide bulk dispersion. Solid polyamide film is ground into small flakes and dispersed in water as a colloidal-like suspension, thus resulting in a pattern of isotropic rings on a 2D SAXS detector. (F) Schematic diagram of 1D scattering intensity profile of polyamide by integrating a 2D SAXS pattern. The profile can be divided into three regions for respective analysis. In the Guinier region, scattering intensity, I, is proportional to the concentration of the system and thus independent of q. In the mass fractal ($I \propto q^{-2-3}$) and the Porod region ($I \propto q^{-3-4}$), the correlation of I with q can provide the structural information of large clusters and small primary units of polyamide chain, respectively.

polyamide film.[59] Further analysis of this WAXS pattern by plotting the scattered intensity *versus* scattering vector, q, suggests the presence of two peaks centered at 1.79 Å^{-1} and 1.22 Å^{-1}. According to Bragg's law ($d = 2\pi/q$), these two peaks correspond to molecular spacings of 3.5 and 5.2 Å, respectively. The 3.5 Å spacing is consistent with "π–π" stacking of aromatic cores (green arrows in Fig. 9D), whereas the 5.2 Å spacing is consistent with the perpendicular packing of aromatic cores in the "T-shaped" configuration (red arrows in Fig. 9D).[59] Based on such WAXS results, researchers revealed the important role of reaction kinetics and post-treatment procedures in affecting the stacking behaviors of aromatic rings. For example, the emerging mLbL IP strategy with well-controlled MPD–TMC reaction leads to the generation of parallel "π–π" stacking, while the conventional IP processes with uncontrolled MPD–TMC reaction give rise to "T-shaped" configurations. It is surmised that the "T-shaped" stacking with loose structure is more favorable for water diffusion, thereby governing the mass transport of polyamide films.

Besides the molecular-level insights from the WAXS measurement of polyamide films, SAXS (or SANS) measurements were used to characterize polyamide dispersions for revealing structural information at the polymer-chain level (Fig. 9E).[60,61] Prior to the scattering experiments, freshly-prepared polyamide films are either loaded into a small quartz capillary,[61] or ground into small flakes and dispersed in water as a colloidal-like suspension.[60] Integration of 2D scattering pattern results in a 1D scattering profile (schematic illustrated in Fig. 9F), which could be divided into three regions for respective analysis.[61] In the Guinier region (extremely low q), scattering intensity, I, is proportional to the concentration of the system and thus independent of q. At a higher q, the correlation of I with q could provide information on polyamide chain structure, including larger clusters or smaller primary units. For example, in the Porod region ($I \propto q^{-3-4}$), the SAXS pattern of an RO polyamide layer reveals that the primary globular units have a radius of ~130 Å, containing ~1500 phenylenediamine trimesamide units.[61] In comparison, the primary unit of an NF polypiperazine layer is slightly smaller, having radii of ~120 Å with ~1400 piperazine trimesamide units.[61] Additionally, a steeper slope for the NF membranes ($\log I/\log q = 3.8$) than that for the RO membranes ($\log I/\log q = 3.4$) suggests that the globular units in the NF membranes have a relatively higher degree of compaction than those in the RO membranes.[61] Notably, the aggregation of these primary units leads to the formation of larger clusters, which could also be characterized by the SAXS

profiles in the mass fractal regions ($I \propto q^{-2-3}$). For instance, the nodular clusters of the NF polypiperazine network have a size of 1900–3000 Å, which is six times larger than that of the RO polyamide network. Taken together, these insights from the scattering studies suggest that the RO polyamide layer has larger primary units, lower chain compaction, and smaller size clusters than those of the NF polypiperazine layer.[60,61] Such differences in the polymer network structures could be related to their desalination performance, thereby facilitating the understanding of the IP reaction for guiding the design of high-performance TFC membranes.

5. Conclusion and outlook

In this Tutorial, we presented a brief history of the development of desalination membranes, discussed the current challenges in the application of conventional TFC membranes, and reviewed emerging progress in IP-based fabrication processes and TFC membrane characterization techniques. Despite extensive research efforts in the past decade, the industrial IP process and its product polyamide layer are largely unchanged since the invention of TFC membranes in the late 1970s, suggesting knowledge gaps between lab research and real-world applications. Herein, we further discuss key limiting factors of the IP process and propose potential research directions for fabricating next-generation TFC desalination membranes.

Development of new IP strategies has been an active area of research in the past decade, as reviewed in this Tutorial. Presently, obtaining a polyamide layer with a smooth surface for fouling control is possible using some emerging approaches, such as electrospray or constructing sacrificial interlayers. However, effective strategies for making membranes with ultrahigh water–salt selectivity are still lacking, mainly owing to the challenges in obtaining a thin, defect-free polyamide film after adjusting reaction conditions of IP. Given the importance of enhanced water–salt selectivity in improving water quality and reducing the cost of desalination, future efforts in developing new IP strategies would require effective measures of molecular-level manipulation of polyamide microstructures where water and solute transport takes place. For example, controlling reaction or posttreatment conditions of IP resulted in different molecular motifs of polyamide, potentially affecting mass transport in TFC membranes.[59] Such insights may lead to new approaches for making high-performance membranes. Notably, advances in materials science related to thin-film fabrication techniques (*e.g.*, self-assembly,[62] atomic layer deposition,[63] and surface-initiated polymerization[64]) can provide new approaches for the design of novel IP strategies.

The use of advanced characterization techniques has enabled substantial progress in the mechanistic understanding of the IP reaction and membrane structure. However, techniques for *in situ* characterization of IP reaction kinetics, as well as *operando* characterization of TFC membranes, are still lacking. As discussed in this Tutorial, the fast kinetics of the IP reaction limit direct observation of polyamide formation. Moreover, the IP reaction involves the generation of heterogeneous environments with both liquid solution and solid polyamide, adding further constraints to the system for *in situ* characterization. For the resulting membranes, existing characterization is largely conducted under ambient conditions, while *operando* characterization of TFC membranes under conditions relevant to real-world operation (*e.g.*, high pressure, crossflow, and salinity) is hampered by numerous technical obstacles. For instance, electron microscopic tools require stringent sample pretreatment (*e.g.*, drying, sectioning, or coating), thereby limiting their uses for *operando* characterization. Although X-ray (or neutron) scattering techniques do not require sample pretreatment, incorporating custom-built setups, which can mimic the operating conditions, into existing facilities is extremely difficult. Given the importance of *in situ* or *operando* information in delineating reaction mechanisms of IP and structure–property–performance relationship of TFC membranes, increasing efforts should be devoted to developing relevant characterization tools and platforms in future research.

In addition to the efforts in developing experimental measures with the required spatial and temporal resolution, molecular simulations can be a versatile tool to gain insights into the IP reaction kinetics and polyamide formation mechanisms. For example, a recent study using molecular dynamic simulation predicted the presence of "π–π" and "T-shaped" stacking for the aromatic rings of the polyamide structure,[65] thereby guiding the selection and design of pertinent characterization tools in revealing such microstructures (see the above section about X-ray scattering techniques).[59] In another simulation study, researchers suggested a reaction-aggregation process of IP in forming small polyamide oligomers, which then aggregated to yield large, solid polyamide clusters to limit further reaction of IP.[66] Notably, their modeling results were also validated by an experimental study,[67] demonstrating the promise of the developed model in studying the complex IP reaction kinetics. Despite such progress, current efforts in the simulation of IP are still in their infancy, largely relying on molecular dynamic simulations.[65,66,68] With recent advances in computation, molecular simulations can play more important roles in understanding IP reaction mechanisms and guiding TFC membrane design. For instance, the utilization of supercomputers can enable more complicated simulations of the IP reaction by taking more reaction factors into consideration. The development of machine learning or artificial intelligence can also relieve researchers of some tedious, time-consuming experiments in finding the best reaction conditions.

Last, in addition to research efforts in academia, the design of IP processes for making next-generation TFC membranes would also require collaborative efforts with the industry. After long-term optimization of the conventional IP process, membrane industries have established an inventory of empirical protocols to making high-performance TFC membranes for different applications, including seawater desalination, wastewater reclamation, or even tap water softening. However, owing to the lack of interactions between academia and industry, a large portion of research efforts in academia still focus on tuning minor conditions of IP to

achieve marginal gains in membrane performance, which may have been realized by industry a long time ago. To avoid such superficial repetition in future research, academic researchers should put more emphasis on revealing IP reaction mechanisms or demonstrating proof-of-concept of new IP strategies, while seeking collaborations with industrial partners in scaling up lab results into commercial products. Such collaborative experiences will enable academic researchers to understand not only the design factors for high-performance membranes, but also the factors that afford scalable production processes.

Conflicts of interest

There are no conflicts to declare.

Acknowledgements

We acknowledge the financial support received from the NSF Nanosystems Engineering Research Center for Nanotechnology-Enabled Water Treatment (EEC-1449500). This work was partly supported by the Fundamental Research Funds for the Central Universities. We also acknowledge fruitful discussions with Wen Ma, Jay Werber, Akshay Deshmukh, and Rhea Verbeke at Yale University.

References

1 M. S. Mauter, I. Zucker, F. Perreault, J. R. Werber, J.-H. Kim and M. Elimelech, The role of nanotechnology in tackling global water challenges, *Nat. Sustain.*, 2018, **1**, 166–175.
2 M. A. Shannon, P. W. Bohn, M. Elimelech, J. G. Georgiadis, B. J. Marinas and A. M. Mayes, Science and technology for water purification in the coming decades, *Nature*, 2008, **452**, 301–310.
3 M. Elimelech and W. A. Phillip, The Future of Seawater Desalination: Energy, Technology, and the Environment, *Science*, 2011, **333**, 712–717.
4 R. Weaver, M. Howells, Y. Yang, S. Lennox and H. Brown, *IDA Water Security Handbook 2019–2020*, 2020.
5 A. Deshmukh, C. Boo, V. Karanikola, S. Lin, A. P. Straub, T. Tong, D. M. Warsinger and M. Elimelech, Membrane distillation at the water-energy nexus: limits, opportunities, and challenges, *Energy Environ. Sci.*, 2018, **11**, 1177–1196.
6 E. Jones, M. Qadir, M. T. H. van Vliet, V. Smakhtin and S.-M. Kang, The state of desalination and brine production: A global outlook, *Sci. Total Environ.*, 2019, **657**, 1343–1356.
7 J. Glater, The early history of reverse osmosis membrane development, *Desalination*, 1998, **117**, 297–309.
8 R. W. Baker, *Membrane Technology and Applications*, Wiley, New York, 2nd edn, 2004.
9 G. M. Geise, H. B. Park, A. C. Sagle, B. D. Freeman and J. E. McGrath, Water permeability and water/salt selectivity tradeoff in polymers for desalination, *J. Membr. Sci.*, 2011, **369**, 130–138.
10 H. B. Park, J. Kamcev, L. M. Robeson, M. Elimelech and B. D. Freeman, Maximizing the right stuff: The trade-off between membrane permeability and selectivity, *Science*, 2017, **356**, eaab0530.
11 J. R. Werber, A. Deshmukh and M. Elimelech, The Critical Need for Increased Selectivity, Not Increased Water Permeability, for Desalination Membranes, *Environ. Sci. Technol. Lett.*, 2016, **3**, 112–120.
12 D. Cohen-Tanugi, R. K. McGovern, S. H. Dave, J. H. Lienhard and J. C. Grossman, Quantifying the potential of ultra-permeable membranes for water desalination, *Energy Environ. Sci.*, 2014, **7**, 1134–1141.
13 X. Zhou, Z. Wang, R. Epsztein, C. Zhan, W. Li, J. D. Fortner, T. A. Pham, J.-H. Kim and M. Elimelech, Intrapore energy barriers govern ion transport and selectivity of desalination membranes, *Sci. Adv.*, 2020, **6**, eabd9045.
14 R. Zhang, Y. Liu, M. He, Y. Su, X. Zhao, M. Elimelech and Z. Jiang, Antifouling membranes for sustainable water purification: strategies and mechanisms, *Chem. Soc. Rev.*, 2016, **45**, 5888–5924.
15 D. Rana and T. Matsuura, Surface Modifications for Antifouling Membranes, *Chem. Rev.*, 2010, **110**, 2448–2471.
16 G.-D. Kang and Y.-M. Cao, Development of antifouling reverse osmosis membranes for water treatment: A review, *Water Res.*, 2012, **46**, 584–600.
17 J. Glater, S. K. Hong and M. Elimelech, The Search for a Chlorine-Resistant Reverse-Osmosis Membrane, *Desalination*, 1994, **95**, 325–345.
18 R. Verbeke, V. Gómez and I. F. J. Vankelecom, Chlorine-resistance of reverse osmosis (RO) polyamide membranes, *Prog. Polym. Sci.*, 2017, **72**, 1–15.
19 Y. Yao, P. Zhang, C. Jiang, R. M. DuChanois, X. Zhang and M. Elimelech, High performance polyester reverse osmosis desalination membrane with chlorine resistance, *Nat. Sustain.*, 2021, **4**, 138–146.
20 S. Karan, Z. Jiang and A. G. Livingston, Sub–10 nm polyamide nanofilms with ultrafast solvent transport for molecular separation, *Science*, 2015, **348**, 1347–1351.
21 X.-H. Ma, Z.-K. Yao, Z. Yang, H. Guo, Z.-L. Xu, C. Y. Tang and M. Elimelech, Nanofoaming of Polyamide Desalination Membranes To Tune Permeability and Selectivity, *Environ. Sci. Technol. Lett.*, 2018, **5**, 123–130.
22 J. R. Werber, C. O. Osuji and M. Elimelech, Materials for next-generation desalination and water purification membranes, *Nat. Rev. Mater.*, 2016, **1**, 16018.
23 Z. Wang, Z. Wang, S. Lin, H. Jin, S. Gao, Y. Zhu and J. Jin, Nanoparticle-templated nanofiltration membranes for ultrahigh performance desalination, *Nat. Commun.*, 2018, **9**, 2004.
24 Z. Yang, P.-F. Sun, X. Li, B. Gan, L. Wang, X. Song, H.-D. Park and C. Y. Tang, A Critical Review on Thin-Film Nanocomposite Membranes with Interlayered Structure: Mechanisms, Recent Developments, and Environmental Applications, *Environ. Sci. Technol.*, 2020, **54**, 15563–15583.
25 S.-J. Park, W. Choi, S.-E. Nam, S. Hong, J. S. Lee and J.-H. Lee, Fabrication of polyamide thin film composite reverse

osmosis membranes via support-free interfacial polymerization, *J. Membr. Sci.*, 2017, **526**, 52–59.

26 Z. Jiang, S. Karan and A. G. Livingston, Water Transport through Ultrathin Polyamide Nanofilms Used for Reverse Osmosis, *Adv. Mater.*, 2018, **30**, 1705973.

27 M. M. Pendergast and E. M. V. Hoek, A review of water treatment membrane nanotechnologies, *Energy Environ. Sci.*, 2011, **4**, 1946–1971.

28 Y. Zhao, C. Qiu, X. Li, A. Vararattanavech, W. Shen, J. Torres, C. Hélix-Nielsen, R. Wang, X. Hu, A. G. Fane and C. Y. Tang, Synthesis of robust and high-performance aquaporin-based biomimetic membranes by interfacial polymerization-membrane preparation and RO performance characterization, *J. Membr. Sci.*, 2012, **423-424**, 422–428.

29 X. Li, S. Chou, R. Wang, L. Shi, W. Fang, G. Chaitra, C. Y. Tang, J. Torres, X. Hu and A. G. Fane, Nature gives the best solution for desalination: Aquaporin-based hollow fiber composite membrane with superior performance, *J. Membr. Sci.*, 2015, **494**, 68–77.

30 C. J. Porter, J. R. Werber, M. Zhong, C. J. Wilson and M. Elimelech, Pathways and Challenges for Biomimetic Desalination Membranes with Sub-Nanometer Channels, *ACS Nano*, 2020, **14**, 10894–10916.

31 E. M. V. Hoek and V. V. Tarabara, *Encyclopedia of membrane science and technology*, Wiley Online Library, 2013.

32 Z. Yang, H. Guo, Z.-K. Yao, Y. Mei and C. Y. Tang, Hydrophilic Silver Nanoparticles Induce Selective Nanochannels in Thin Film Nanocomposite Polyamide Membranes, *Environ. Sci. Technol.*, 2019, **53**, 5301–5308.

33 J. Yin, Z. Yang, C. Y. Tang and B. Deng, Probing the Contributions of Interior and Exterior Channels of Nanofillers toward the Enhanced Separation Performance of a Thin-Film Nanocomposite Reverse Osmosis Membrane, *Environ. Sci. Technol. Lett.*, 2020, **7**, 766–772.

34 M. Mulder, *Basic Principles of Membrane Technology*, Kluwer Academic Pulisher, The Netherlands, 2nd edn, 1996.

35 R. J. Petersen, Composite Reverse-Osmosis and Nanofiltration Membranes, *J. Membr. Sci.*, 1993, **83**, 81–150.

36 J. Liu, D. Hua, Y. Zhang, S. Japip and T.-S. Chung, Precise Molecular Sieving Architectures with Janus Pathways for Both Polar and Nonpolar Molecules, *Adv. Mater.*, 2018, **30**, 1705933.

37 M. J. T. Raaijmakers and N. E. Benes, Current trends in interfacial polymerization chemistry, *Prog. Polym. Sci.*, 2016, **63**, 86–142.

38 A. F. Ismail, M. Padaki, N. Hilal, T. Matsuura and W. J. Lau, Thin film composite membrane—Recent development and future potential, *Desalination*, 2015, **356**, 140–148.

39 Z. Tan, S. Chen, X. Peng, L. Zhang and C. Gao, Polyamide membranes with nanoscale Turing structures for water purification, *Science*, 2018, **360**, 518–521.

40 Y. Liang, Y. Zhu, C. Liu, K.-R. Lee, W.-S. Hung, Z. Wang, Y. Li, M. Elimelech, J. Jin and S. Lin, Polyamide nanofiltration membrane with highly uniform sub-nanometre pores for sub-1 Å precision separation, *Nat. Commun.*, 2020, **11**, 2015.

41 X. Lu, S. Nejati, Y. Choo, C. O. Osuji, J. Ma and M. Elimelech, Elements Provide a Clue: Nanoscale Characterization of Thin-Film Composite Polyamide Membranes, *ACS Appl. Mater. Interfaces*, 2015, **7**, 16917–16922.

42 G. Joung-Eun, L. Seunghye, C. M. Stafford, L. J. Suk, C. Wansuk, K. Bo-Young, B. Kyung-Youl, E. P. Chan, C. J. Young, B. Joona and L. Jung-Hyun, Molecular Layer-by-Layer Assembled Thin-Film Composite Membranes for Water Desalination, *Adv. Mater.*, 2013, **25**, 4778–4782.

43 J. Fenn, M. Mann, C. Meng, S. Wong and C. Whitehouse, Electrospray ionization for mass spectrometry of large biomolecules, *Science*, 1989, **246**, 64–71.

44 M. R. Chowdhury, J. Steffes, B. D. Huey and J. R. McCutcheon, 3D printed polyamide membranes for desalination, *Science*, 2018, **361**, 682–686.

45 X.-H. Ma, Z. Yang, Z.-K. Yao, H. Guo, Z.-L. Xu and C. Y. Tang, Interfacial Polymerization with Electrosprayed Microdroplets: Toward Controllable and Ultrathin Polyamide Membranes, *Environ. Sci. Technol. Lett.*, 2018, **5**, 117–122.

46 Z. Yang, H. Guo and C. Y. Tang, The upper bound of thin-film composite (TFC) polyamide membranes for desalination, *J. Membr. Sci.*, 2019, **590**, 117297.

47 P. S. Singh, A. P. Rao, P. Ray, A. Bhattacharya, K. Singh, N. K. Saha and A. V. R. Reddy, Techniques for characterization of polyamide thin film composite membranes, *Desalination*, 2011, **282**, 78–86.

48 V. Freger, A. Bottino, G. Capannelli, M. Perry, V. Gitis and S. Belfer, Characterization of novel acid-stable NF membranes before and after exposure to acid using ATR-FTIR, TEM and AFM, *J. Membr. Sci.*, 2005, **256**, 134–142.

49 C. Y. Tang, Y.-N. Kwon and J. O. Leckie, Probing the nano- and micro-scales of reverse osmosis membranes—A comprehensive characterization of physiochemical properties of uncoated and coated membranes by XPS, TEM, ATR-FTIR, and streaming potential measurements, *J. Membr. Sci.*, 2007, **287**, 146–156.

50 M. M. Kłosowski, C. M. McGilvery, Y. Li, P. Abellan, Q. Ramasse, J. T. Cabral, A. G. Livingston and A. E. Porter, Micro-to nano-scale characterisation of polyamide structures of the SW30HR RO membrane using advanced electron microscopy and stain tracers, *J. Membr. Sci.*, 2016, **520**, 465–476.

51 F. Pacheco, R. Sougrat, M. Reinhard, J. O. Leckie and I. Pinnau, 3D visualization of the internal nanostructure of polyamide thin films in RO membranes, *J. Membr. Sci.*, 2016, **501**, 33–44.

52 T. E. Culp, Y.-X. Shen, M. Geitner, M. Paul, A. Roy, M. J. Behr, S. Rosenberg, J. Gu, M. Kumar and E. D. Gomez, Electron tomography reveals details of the internal microstructure of desalination membranes, *Proc. Natl. Acad. Sci. U. S. A.*, 2018, **115**, 8694–8699.

53 T. E. Culp, B. Khara, K. P. Brickey, M. Geitner, T. J. Zimudzi, J. D. Wilbur, S. D. Jons, A. Roy, M. Paul, B. Ganapathysubramanian, A. L. Zydney, M. Kumar and E. D. Gomez, Nanoscale control of internal inhomogeneity

enhances water transport in desalination membranes, *Science*, 2021, **371**, 72–75.

54 O. Coronell, B. J. Marinas, X. J. Zhang and D. G. Cahill, Quantification of functional groups and modeling of their ionization behavior in the active layer of FT30 reverse osmosis membrane, *Environ. Sci. Technol.*, 2008, **42**, 5260–5266.

55 D. Chen, J. R. Werber, X. Zhao and M. Elimelech, A facile method to quantify the carboxyl group areal density in the active layer of polyamide thin-film composite membranes, *J. Membr. Sci.*, 2017, **534**, 100–108.

56 R. Verbeke, A. Bergmaier, S. Eschbaumer, H. Mariën, G. Dollinger and I. F. J. Vankelecom, Full elemental depth-profiling with nanoscale resolution: The potential of Elastic Recoil Detection (ERD) in membrane science, *J. Membr. Sci.*, 2019, **572**, 102–109.

57 S. H. Kim, S.-Y. Kwak and T. Suzuki, Positron Annihilation Spectroscopic Evidence to Demonstrate the Flux-Enhancement Mechanism in Morphology-Controlled Thin-Film-Composite (TFC) Membrane, *Environ. Sci. Technol.*, 2005, **39**, 1764–1770.

58 T. Fujioka, N. Oshima, R. Suzuki, W. E. Price and L. D. Nghiem, Probing the internal structure of reverse osmosis membranes by positron annihilation spectroscopy: Gaining more insight into the transport of water and small solutes, *J. Membr. Sci.*, 2015, **486**, 106–118.

59 Q. Fu, N. Verma, H. Ma, F. J. Medellin-Rodriguez, R. Li, M. Fukuto, C. M. Stafford, B. S. Hsiao and B. M. Ocko, Molecular Structure of Aromatic Reverse Osmosis Polyamide Barrier Layers, *ACS Macro Lett.*, 2019, **8**, 352–356.

60 P. S. Singh and V. K. Aswal, Compacted Nanoscale Blocks To Build Skin Layers of Reverse Osmosis and Nanofiltration Membranes: A Revelation from Small-Angle Neutron Scattering, *J. Phys. Chem. C*, 2007, **111**, 16219–16226.

61 P. S. Singh, P. Ray, Z. Xie and M. Hoang, Synchrotron SAXS to probe cross-linked network of polyamide 'reverse osmosis' and 'nanofiltration' membranes, *J. Membr. Sci.*, 2012, **421-422**, 51–59.

62 X. Feng, Q. Imran, Y. Zhang, L. Sixdenier, X. Lu, G. Kaufman, U. Gabinet, K. Kawabata, M. Elimelech and C. O. Osuji, Precise nanofiltration in a fouling-resistant self-assembled membrane with water-continuous transport pathways, *Sci. Adv.*, 2019, **5**, eaav9308.

63 X. Zhou, Y.-Y. Zhao, S.-R. Kim, M. Elimelech, S. Hu and J.-H. Kim, Controlled TiO2 Growth on Reverse Osmosis and Nanofiltration Membranes by Atomic Layer Deposition: Mechanisms and Potential Applications, *Environ. Sci. Technol.*, 2018, **52**, 14311–14320.

64 B. Liang, H. Wang, X. Shi, B. Shen, X. He, Z. A. Ghazi, N. A. Khan, H. Sin, A. M. Khattak, L. Li and Z. Tang, Microporous membranes comprising conjugated polymers with rigid backbones enable ultrafast organic-solvent nanofiltration, *Nat. Chem.*, 2018, **10**, 961–967.

65 T. Wei, L. Zhang, H. Zhao, H. Ma, M. S. J. Sajib, H. Jiang and S. Murad, Aromatic Polyamide Reverse-Osmosis Membrane: An Atomistic Molecular Dynamics Simulation, *J. Phys. Chem. B*, 2016, **120**, 10311–10318.

66 J. Muscatello, E. A. Müller, A. A. Mostofi and A. P. Sutton, Multiscale molecular simulations of the formation and structure of polyamide membranes created by interfacial polymerization, *J. Membr. Sci.*, 2017, **527**, 180–190.

67 F. Foglia, S. Karan, M. Nania, Z. Jiang, A. E. Porter, R. Barker, A. G. Livingston and J. T. Cabral, Neutron Reflectivity and Performance of Polyamide Nanofilms for Water Desalination, *Adv. Funct. Mater.*, 2017, **27**, 1701738.

68 V. Kolev and V. Freger, Hydration, porosity and water dynamics in the polyamide layer of reverse osmosis membranes: A molecular dynamics study, *Polymer*, 2014, **55**, 1420–1426.